Journal of Physics: Conference Series **2462** (2023) 012060 doi:10.1088/1742-6596/2462/1/012060

Enhancement of superconductivity at a quantum critical point in $(Ca_xSr_{1-x})_3Rh_4Sn_{13}$

J A Krieger[1,*], Z Guguchia[1], R Khasanov[1], P K Biswas[1], L Li[2,†] K Wang[2,‡], C Petrovic[2], and E Morenzoni[1]

[1] Laboratory for Muon Spin Spectroscopy, Paul Scherrer Institute, CH-5232 Villigen PSI, Switzerland

[2] Condensed Matter Physics and Materials Science Department, Brookhaven National Laboratory, Upton, New York 11973, USA

[*] Current address: Max Planck Institute of Microstructure Physics, Weinberg 2, 06120 Halle, Germany

[†] Current address: School of Physics Science and Technology, GuangXi University.

[‡] Current address: Department of Physics, University of Maryland, College Park, Maryland 20742-4111, USA

E-mail: elvezio.morenzoni@psi.ch

Abstract. We report microscopic studies by muon spin spectroscopy of the superconducting properties as a function of chemical and hydrostatic pressure in the cubic ternary intermetallic $(Ca_xSr_{1-x})_3Rh_4Sn_{13}$ compounds. We find evidence of a quantum critical point at a critical pressure p_c in the superconducting phase, where the superfluid density increases by a factor of two and the superconducting pairing strength displays a pronounced maximum. The enhancement of superconductivity is related to the structural phase transition at p_c, which is accompanied by profound changes of the Fermi surface associated to the suppression of a charge density wave (CDW). The quantum critical point separates a superconducting phase coexisting with CDW from a pure superconducting phase, while in both phases superconductivity has a strong-coupling phonon-mediated BCS-like *s*-wave character. Together with the related isoelectronic compound $(Ca_xSr_{1-x})_3Ir_4Sn_{13}$, this system shows that conventional BCS superconductors in the presence of competing orders may display behaviour and characteristics of unconventional superconductors.

1. Introduction

The interaction and interplay between superconductivity, structural or other types of electronic order is matter of ongoing research and remains one of the fundamental subjects of condensed matter and material science. In a variety of systems, ranging from organic materials, heavy fermions, through cuprate and Fe-based high T_c superconductors, many common features are found, in spite of different structural and physical properties. This is apparent in the phase diagrams, where critical temperatures or order parameters are expressed as a function of some tuning parameters, such as doping, magnetic field or pressure [1, 2, 3, 4].

Remeika phase materials with the generic formula $R_3T_4X_{13}$ and a cubic structure have attracted particular interest because they display a large variety of phenomena, which are also found in exotic and unconventional superconductors. A broad variety of elements can be chosen for the different sites, where e.g. R can be a rare-earth, alkaline earth element

or also an actinide such as Th, T is a transition metal, and X is a group IV element, usually Ge or Sn [5, 6]. In particular, the stannide compounds $(Ca_xSr_{1-x})_3Ir_4Sn_{13}$ and the isoelectronic $(Ca_xSr_{1-x})_3Rh_4Sn_{13}$ have focused the interest because they simultaneously display superconductivity and a structural phase transition at a temperature T^* accompanied by profound changes in the Fermi surface indicative of the formation of a charge density wave (CDW) [7, 8, 9, 10, 11, 12, 13, 14, 15]. The structural transition has a clear signature in XRD [7, 14] and coincides with anomalies in many properties of the electronic system which manifest in transport, thermal, magnetic and optical measurements [10, 13, 15, 14, 16, 17, 18, 19, 20]. This suggests that the structural transition is occurring via the formation of a CDW. The role and interaction of superconductivity/CDW/structural transitions is central also in cuprates superconductors, where after the discovery of the competition between CDW and superconductivity in $YBa_2Cu_3O_{6.67}$ [21], other different types of CDW have been found and where the presence of a CDW appears to be generic [1]. In this context the regions in the vicinity of the phase transition and quantum critical points (QCPs) are of particular interest [22]. As shown in Refs. [7, 14] the ternary metallic stannides offer a playground to study the interplay of these order parameters, without being affected by spin fluctuations from a nearby magnetic transition. Local investigations of the evolution of the superconducting state as a function of pressure in $(Ca_xSr_{1-x})_3Ir_4Sn_{13}$ found s-wave superconductivity with strong enhancement of the superfluid density and of the coupling strength as expressed by the $R \equiv \Delta(0)/(k_BT_c)$ ratio at 1.6 GPa, thus presenting direct evidence of the presence of a quantum critical point at the end point of the structural/CDW phase transition, separating two superconducting phases, one coexisting with CDW (below p_c) and another above [23, 24, 25]. At the same time, evidence of a QCP in $(Ca_xSr_{1-x})_3Rh_4Sn_{13}$ was observed through phonon-softening [26] a peak in the critical current [27] and by specific heat studies finding an increase of R and a decrease of the Debye frequency [16]. Furthermore, based on the effect of disorder in $Ca_3Rh_4Sn_{13}$, a singlet, multiband, A_{1g}^{+-} state with an s^{+-} gap has been proposed as the most likely order parameter [28].

Here, we use muon spin spectroscopy (μSR) to characterise at a local level the superconducting and magnetic properties of $(Ca_xSr_{1-x})_3Rh_4Sn_{13}$ as a function of chemical (by substitution of Sr with Ca) in combination with hydrostatic pressure and investigate how the microscopic superconducting parameters evolve. The effective magnetic penetration depth $\lambda(T,p)$ which is a measure of the superfluid density $\lambda^{-2} \propto \rho_s \equiv \frac{n_s}{m^*}$ (where n_s is the supercarrier density and m^* effective mass), is determined as a function of pressure and temperature from the inhomogeneous field distribution $p(B)$, which characterises the formation of the vortex state in a field cooled measurement. From its temperature dependence the symmetry and the $T = 0$ K characteristics of the superconducting state are determined. This allows to study their evolution around the QCP $T^* \cong 0$K. Our experiment shows that the superfluid density of $(Ca_xSr_{1-x})_3Rh_4Sn_{13}$ doubles and that R reaches a maximum at p_c. Similarly to $(Ca_xSr_{1-x})_3Ir_4Sn_{13}$, the $(Ca_xSr_{1-x})_3Rh_4Sn_{13}$ samples remain conventional electron-phonon mediated s-wave superconductors across the QCP and the significant increase of paired carriers and coupling strength is related to the suppression of the CDW and concomitant phonon softening at the QCP.

2. Experiment

2.1. Experimental Details

Single crystals of $(Ca_xSr_{1-x})_3Rh_4Sn_{13}$ were grown from excess Sn. Elemental Ca_xSr_{1-x}, Rh and Sn in 3:4:93 atomic ratio were placed in an alumina crucible and sealed under vacuum in a quartz ampule along with some quartz wool for filtration. The ampule was heated up to 1100 °C, kept for six hours, fast cooled to 800 °C and then slow cooled to 490 °C where the excess Sn was decanted in a centrifuge outside the furnace [12].

The complete substitution of Ca with Sr corresponds to a negative pressure of −6.8 GPa [14].

Combining partial Ca/Sr substitution with hydrostatic pressure, the pressure range from −3.9 GPa to 1.9 GPa has been investigated, where zero pressure corresponds to the non-pressurised $Ca_3Rh_4Sn_{13}$ compound. To measure the microscopic properties of the superconducting state, transverse-field (TF) μSR experiments were performed on different instrument of the SμS facility the Paul Scherrer Institute (Villigen, Switzerland). The instruments Dolly and GPS with a 28 MeV/c surface muon beam were used for low background measurements on non-pressurized samples [29], whereas the GPD instrument making use of high energy muons ($\sim$ 100 MeV/c) at the μE1 decay channel beamline allowed to perform μSR studies under pressure [30, 31]. Forward and backward positron detectors with respect to the initial muon polarization were used for the measurements of the μSR asymmetry time spectrum $A(t)$. For the experiments under hydrostatic pressure we followed the procedure described in detail in Ref. [25]. In this case several (single crystal) pieces of the compound were loaded into the cylindrical pressure cell. The sample dimensions were chosen to maximize the filling factor of the pressure cell (diameter 6 mm, height 15 mm). A piston-cylinder pressure cell was used with Daphne oil as a pressure-transmitting medium. Measurements under pressure in the $x = 1$, ($x = 0.84$) sample were performed in a CuBe (MP35) pressure cell, respectively. The pressure was calibrated by measuring via AC susceptibility the superconducting transition of a very small indium plate inserted in the cell. The fraction of the muons stopping in the sample was approximately 40 % with the CuBe cell and 35 % with the MP35N cell. The ambient pressure measurement on the $x = 1$ and $x = 0.84$ were performed with different instruments and pressure cells to better assess the background contribution arising from muons stopping in the cell walls and confirm the consistency of the results. In addition, resistivity and magnetoresistance measurements to determine $\rho(T)$ and $B_{c2}(T)$ were performed using a PPMS *Quantum Design* instrument.

2.2. Data analysis

Muon spin rotation (μSR) measurements in the vortex state have been performed as a function of increasing temperature after initial field-cooling of the sample. Representative time spectra on $(Ca_xSr_{1-x})_3Rh_4Sn_{13}$ in the normal and superconducting state at different hydrostatic pressures and chemical compositions are shown in Fig. 1. These spectra yield information about the superconducting properties. For instance, the average muon spin precession frequency is directly proportional to the average local magnetic field at the muon site and thus reflects the diamagnetic shift associated with the vortex supercurrents. In the vortex state the precession is damped and the damping is determined by the width of the field distribution, which depends on the characteristic length scales of the superconductor. The measured asymmetry has contributions from both the sample signal and background $A(t) = A_s(t) + A_{bg}(t)$. In the measurements with a pressure cell the background is particularly pronounced, since a significant number of the muons stop inside of the cell. This background can be clearly seen as a beating between between the oscillations from the two contributions, Fig. 1a,b. Such a beating is absent in measurements at Dolly and GPS where the background contribution is much smaller, Fig. 1(c,d). The spectral evolution of the background slightly depends on the type of pressure cell and for the CuBe and MP35 piston anvil cells used here, it can be modelled by the following functions [32, 25]:

$$A_{\mathrm{CuBe}}(t) = A_{\mathrm{cell}} \exp\left(-\frac{\sigma^2_{\mathrm{CuBe}} t^2}{2}\right) \cos(\gamma_\mu B_{\mathrm{cell}} t + \varphi) \tag{1}$$

$$A_{\mathrm{MP35}}(t) = A_{\mathrm{cell}} \exp\left(-\frac{\sigma^2_{\mathrm{MP35}} t^2}{2}\right) \mathrm{e}^{-\lambda_{\mathrm{MP35}} t} \cos(\gamma_\mu B_{\mathrm{cell}} t + \varphi), \tag{2}$$

where A_{cell} depends on the portion of muons stopping in the pressure cell, φ is the initial muon spin phase, and the Gaussian accounts for depolarisation by nuclear moments. In the MP35

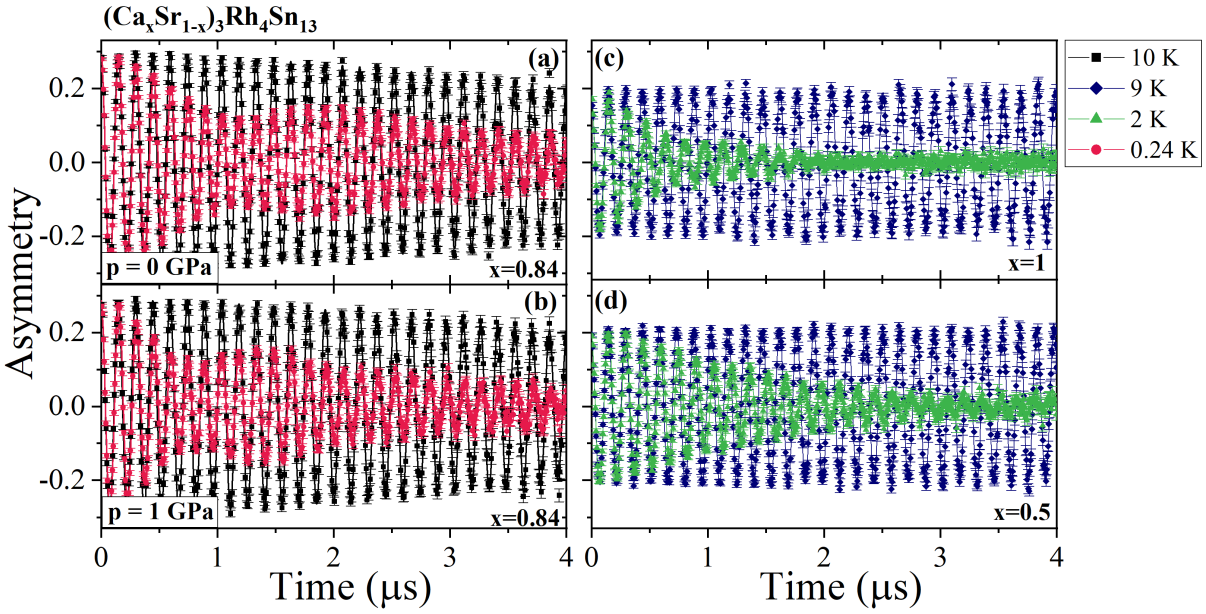

Figure 1. Comparison of μSR time spectra above and below T_c, for different $(Ca_xSr_{1-x})_3Rh_4Sn_{13}$ compositions x and pressures. **(a)** Ambient pressure and **(b)** 1 GPa measurements on the $x = 0.84$ sample in a CuBe pressure cell. **(c,d)** Ambient pressure measurements without pressure cell on the $x = 1$ and $x = 0.5$ samples, respectively.

pressure cell there is an additional dynamic contribution leading to an an exponential relaxation with rate λ_{MP35}. Note that this dynamic contribution becomes strongly temperature dependent at low temperature, which cannot be reliably disentangled from the sample's temperature dependence. Therefore, only measurements above 2 K have been considered in the MP35 pressure cell. Below the superconducting transition, the field distribution in the pressure cell is further affected by the magnetic fields arising from the diamagnetism of the sample. To account for this, the change in the mean field B_{cell} and depolarization rate $\sigma_{CuBe/MP35}$ of the pressure cell was assumed to be proportional to the field shift in the sample [33].

In the superconducting state, the field distribution of the sample is well represented by a sum of several (n) Gaussians [34, 35, 36]:

$$A(t) = A_0 \sum_{i=1}^{n} r_i \exp\left(-\frac{\sigma_i^2 t^2}{2}\right) \cos(\gamma_\mu B_i t + \varphi), \tag{3}$$

$$\langle B \rangle = \sum_{i=1}^{n} r_i B_i \quad ; \qquad \frac{\sigma^2}{\gamma_\mu^2} := \langle \Delta B^2 \rangle = \sum_{i=1}^{n} r_i \left[\left(\frac{\sigma_i}{\gamma_\mu}\right)^2 + (B_i - \langle B \rangle)^2 \right] \tag{4}$$

where A_0 is the initial sample asymmetry, $r_i \in (0,1)$, $\sum_{i=1}^{n} r_i = 1$, and $\langle B \rangle$ and $\langle \Delta B \rangle$ describe the first and second moment of the field distribution. In this case it was sufficient to use $n = 2$ below T_c and $n = 1$ above.

The superconducting contribution to the second moment of the field distribution $\sigma_{sc} = \sqrt{\sigma^2 - \sigma_n^2}$ has been obtained by subtracting the contribution from nuclear moments σ_n, which is determined above T_c. This width of the superconducting field distribution reflects the number and size of vortices in the sample and thereby the magnetic penetration depth. Within an analytical approximation of a hexagonal Ginzburg-Landau vortex lattice, this relationship can

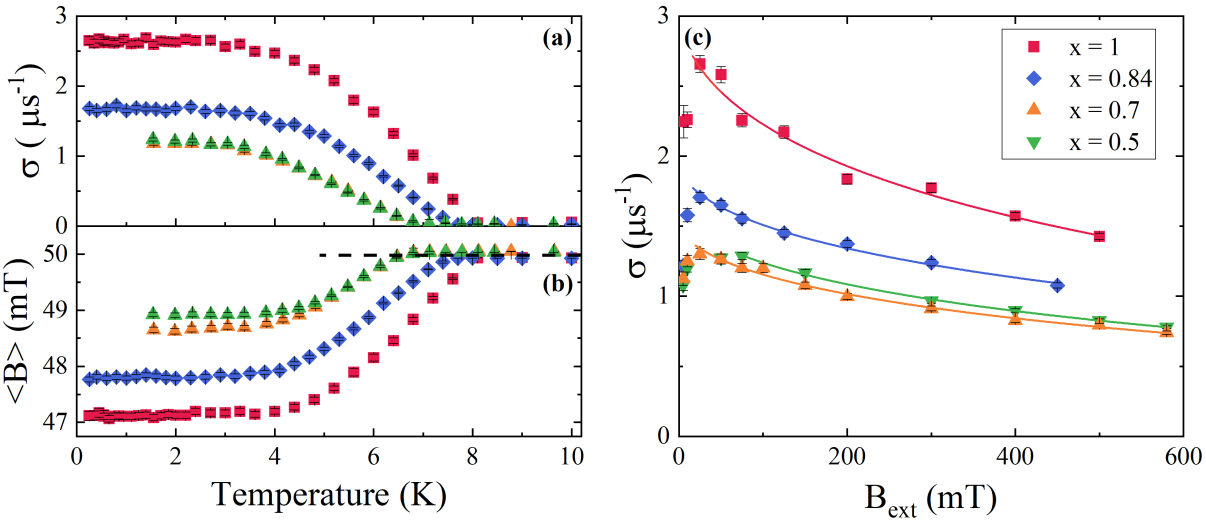

Figure 2. Temperature dependence of **(a)** depolarization rate and **(b)** mean field for the different samples at ambient pressure in a field of 50 mT. **(c)** Applied field dependence under field-cooling conditions of the depolarization rate at a temperature of 1.6 K. The solid lines show fits of Eq. 5 from the main text.

be parameterised as [37]:

$$\sigma_{sc}\left[\mu s^{-1}\right] = 4.854 \times 10^4 (1-b)\left[1 + 1.21\left(1-\sqrt{b}\right)^3\right]\lambda\,[\mathrm{nm}]^{-2}, \tag{5}$$

where $b := \langle B\rangle / B_{c2}$ is the reduced magnetic field.

3. Results

The ambient pressure dependence of the first and second moment of the magnetic field distribution in an applied transverse field of 50 mT $> \mu_0 H_{c1}$ is shown in Fig. 2(a). Below the superconducting transition temperature we find a pronounced, order-parameter like increase (decrease) of σ (B) indicating the formation of the vortex lattice. We note that the μSR signal is consistent with the full sample asymmetry being affected by superconductivity at all temperatures and pressures below T_c, which indicates the absence of any microscopic phase separation.

As a function of increasing applied field at 1.6 K the width of the field distribution σ first increases, as more vortices are penetrating the sample and then decreases towards higher field, as the vortices become closer to each other, Fig. 2(b). At fields above where σ is maximal, the field dependence is well described by Eq. 5, which is shown as a solid line in Fig. 2(b). This motivates the use of Eq. 5 to determine the temperature dependence of λ. For this purpose, the reduced field was calculated based on the values of B_{c2} measured with resistivity down to 2 K at ambient pressure, which was interpolated linearly as a function of temperature and combined hydrostatic and chemical pressure. Note that at low temperature $\langle B\rangle \cong B_{\mathrm{ext}} \ll B_{c2}(T=0)$ and thus, any deviation from B_{c2} from the assumed linear behavior at low temperature would have little influence on the determined values of λ.

The resulting temperature dependence of λ^{-2} at different hydrostatic pressures which is a measure of the superfluid density is shown in Fig. 3. We find that λ^{-2} increases sharply at T_c, but then saturates at low temperature. This is a clear indication, that the pairing wave function

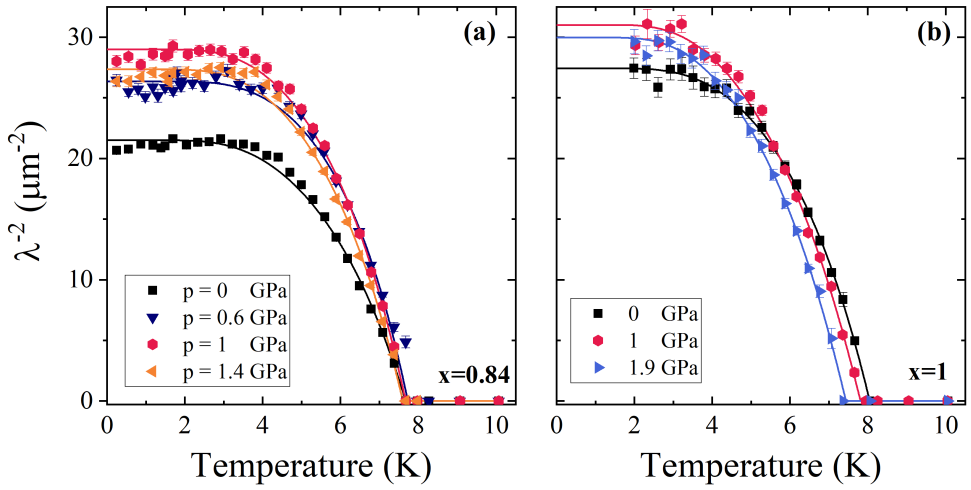

Figure 3. Temperature dependence of the superfluid density at different hydrostatic pressures in the **(a)** $x = 0.84$ and **(b)** $x = 1$ samples.

in $(Ca_xSr_{1-x})_3Rh_4Sn_{13}$ is fully gapped, whereas the superfluid density would be expected to increase with decreasing temperature for nodal superconductivity. Indeed, at all pressures and temperatures, the superfluid density is well modelled by a s-wave BCS-like gap [38]

$$\lambda^{-2}(T) = \lambda_0^{-2}\left[1 - 2\int_{\Delta}^{\infty}\left(-\frac{\partial f}{\partial E}\right)\frac{E}{\sqrt{E^2 - \Delta(T)^2}}\mathrm{d}E\right] \tag{6}$$

where f is the Fermi function and the temperature dependence of the gap is approximated by [39]:

$$\Delta(T) = \Delta_0 \tanh\left\{1.82\left[1.018\left(\frac{T}{T_c} - 1\right)\right]^{0.51}\right\}. \tag{7}$$

This parametrization allows to fit the gap as a function of T_c, λ_0 and Δ_0, which are shown in Fig. 4 and the corresponding curves drawn as solid lines in Fig. 3 are in very good agreement with the data. However, note that the gap to T_c ratio needs to be treated as an adjustable parameter [40], and converges to a value significantly larger than the BCS ratio of ~ 1.76 at all compositions and pressures, Fig. 4(c). This implies the presence of strong coupling superconductivity, similar to what has been observed in $Sr_3Ir_4Sn_{13}$ [23] and $Ca_3Ir_4Sn_{13}$ [24, 25].

4. Discussion

There is a strong increase of the superfluid density across the quantum phase transition from $\lambda^{-2} = 14.7(3)\,\mu\mathrm{m}^{-2}$ to $\lambda^{-2} = 29(2)\,\mu\mathrm{m}^{-2}$, corresponding to an increase of the superfluid density by almost 100 %, Fig. 4(b). This is a clear signature that the charge density wave phase is competing with the coexisting superconductive phase for the available conduction electrons. A suppression of the density of states at the Fermi-level in the Sn 5s band by 13 % at the CDW transition has been observed in ^{119}Sn NMR measurements on $Sr_3Rh_4Sn_{13}$ [15]. Assuming the density of states of a free electron gas $N(E_F) \propto n^{1/3}$, this could only account for an increase in the charge carrier density in this band by $\approx 44\,\%$. However the superfluid density is also inversely proportional to the effective mass $m^* = m_b(1 + \lambda_{e-ph})$ which might change across the phase transition. Considering such an additional change of the electron phonon coupling, which increases from $\lambda_{e-ph} = 0.936$ in $Sr_3Rh_4Sn_{13}$ [41] to $\lambda_{e-ph} = 1.622$ in $Ca_3Rh_4Sn_{13}$ [42], this could

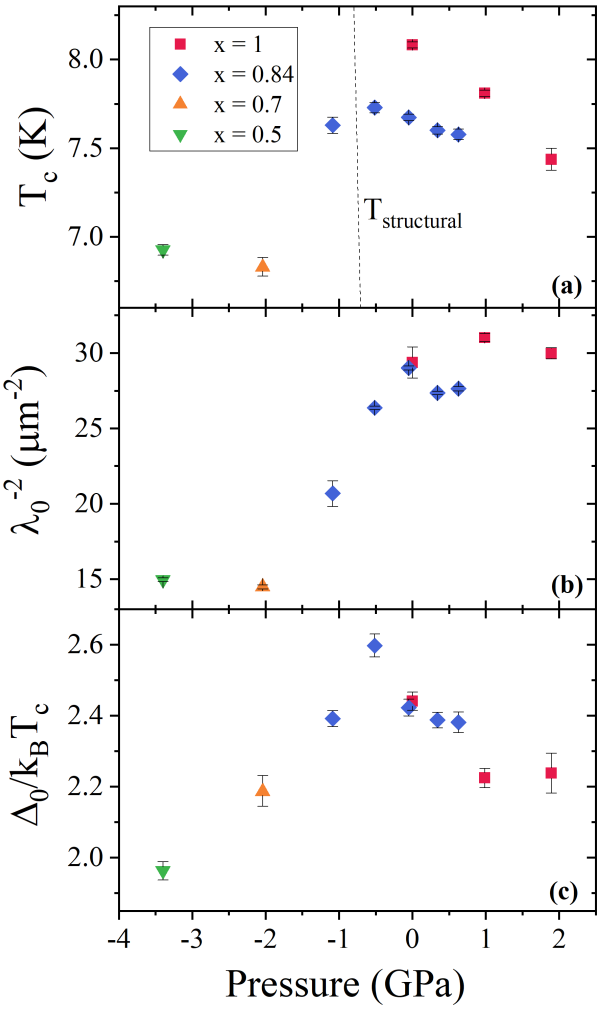

Figure 4. Combined hydrostatic and chemical pressure dependence of **(a)** the transition temperature T_c, **(b)** superfluid density at $T = 0\,\mathrm{K}$ and **(c)** $\Delta_0/k_\mathrm{B}T_c$.

explain the observed behaviour. Also, note that in the pristine $Ca_3Rh_4Sn_{13}$ at ambient pressure we find that $\lambda(0) = 179.5(3)\,\mathrm{nm}$ is significantly smaller than the $\lambda(0) = 330\,\mathrm{nm}$ observed in irradiated samples [28].

The ratio between the gap at zero temperature and the superconducting transition temperature shown in Figure 4(c) peaks near the QCP, concomitant with the phonon softening associated with the suppression of the CDW. The same behaviour has already been found in heat capacity measurements [16]. However, the values found in our microscopic measurement are significantly lower than the ones obtained from the electronic specific heat data, which are sensitive to the subtraction of the phonon contribution [16]. Also note that the gap-to-T_c ratio in $Ca_3Ir_4Sn_{13}$ exceeds the maximum possible value of 2.77 possible within the framework of strong coupling Eliashberg theory [43], which has been attributed to the presence of additional low-energy phonon modes at the QCP which enhance the coupling strength [25]. Here the coupling strength remains below this value at all pressures.

In conclusion, we find clear signatures of a pressure tuned QCP in $(Ca_xSr_{1-x})_3Rh_4Sn_{13}$, which is hallmarked by a significant increase in superconducting carriers and a peak in the

coupling strength, while keeping a fully gapped, strong coupling BCS-like character across the whole phase diagram.

5. Acknowledgement

This work is based on experiments performed at the Swiss Muon Source (SμS), Paul Scherrer Institute, Villigen, Switzerland. The work at PSI was supported by the Swiss National Science Foundation and work at Brookhaven was supported by the U.S. DOE under Contract No. DE-SC00112704.

References

[1] Keimer B, Kivelson S A, Norman M R, Uchida S and Zaanen J 2015 *Nature* **518** 179–186
[2] Paglione J and Greene R L 2010 *Nature Physics* **6** 645–658
[3] Scalapino D J 2012 *Reviews of Modern Physics* **84** 1383–1417
[4] Fradkin E, Kivelson S A and Tranquada J M 2015 *Reviews of Modern Physics* **87** 457–482
[5] Remeika J P, Espinosa G P, Cooper A S, Barz H, JM Rowell, McWhan D B, Vandenberg J M, Moncton D E, Z Fisk, Woolf L D, Hamaker H C, Maple M B, Shirane G and Thomlinson W 1980 *Solid State Communications* **34** 923 – 926
[6] Espinosa G P 1980 *Materials Research Bulletin* **15** 791 – 798
[7] Klintberg L E, Goh S K, Alireza P L, Saines P J, Tompsett D A, Logg P W, Yang J, Chen B, Yoshimura K and Grosche F M 2012 *Physical Review Letters* **109** 237008
[8] Zhou S Y, Zhang H, Hong X C, Pan B Y, Qiu X, Dong W N, Li X L and Li S Y 2012 *Physical Review B* **86** 064504
[9] Mazzone D G, Gerber S, Gavilano J L, Sibille R, Medarde M, Delley B, Ramakrishnan M, Neugebauer M, Regnault L P, Chernyshov D, Piovano A, Fernández-Díaz T M, Keller L, Cervellino A, Pomjakushina E, Conder K and Kenzelmann M 2015 *Physical Review B* **92** 024101
[10] Kuo C N, Liu H F, Lue C S, Wang L M, Chen C C and Kuo Y K 2014 *Physical Review B* **89** 094520
[11] Wang L M, Wang C Y, Chen G M, Kuo C N and Lue C S 2015 *New Journal of Physics* **17** 033005
[12] Wang K and Petrovic C 2012 *Physical Review B* **86** 024522
[13] Fang A F, Wang X B, Zheng P and Wang N L 2014 *Physical Review B* **90** 035115
[14] Goh S K, Tompsett D A, Saines P J, Chang H C, Matsumoto T, Imai M, Yoshimura K and Grosche F M 2015 *Physical Review Letters* **114** 097002
[15] Kuo C N, Tseng C W, Wang C M, Wang C Y, Chen Y R, Wang L M, Lin C F, Wu K K, Kuo Y K and Lue C S 2015 *Physical Review B* **91** 165141
[16] Yu W C, Cheung Y W, Saines P J, Imai M, Matsumoto T, Michioka C, Yoshimura K and Goh S K 2015 *Physical Review Letters* **115** 207003
[17] Ban W J, Wang H P, Tseng C W, Kuo C N, Lue C S and Wang N L 2017 *Science China Physics, Mechanics & Astronomy* **60** 047011
[18] Tseng C W, Kuo C N, Li B S, Wang L M, Gippius A A, Kuo Y K and Lue C S 2018 *Solid State Communications* **270** 26–29
[19] Luo J, Yang J, Maeda S, Li Z and Zheng G Q 2018 *Chinese Physics B* **27** 077401
[20] Terasaki Y, Yamaguchi R, Ishii Y, Tada Y, Yamamoto A and Mori S 2021 *Journal of the Physical Society of Japan* **90** 113704
[21] Chang J, Blackburn E, Holmes A T, Christensen N B, Larsen J, Mesot J, Liang R, Bonn D A, Hardy W N, Watenphul A, Zimmermann M v, Forgan E M and Hayden S M 2012 *Nature Physics* **8** 871–876
[22] Coleman P and Schofield A J 2005 *Nature* **433** 226–229
[23] Biswas P K, Amato A, Khasanov R, Luetkens H, Wang K, Petrovic C, Cook R M, Lees M R and Morenzoni E 2014 *Physical Review B* **90** 144505
[24] Biswas P K, Amato A, Wang K, Petrovic C, Khasanov R, Luetkens H and Morenzoni E 2014 *Journal of Physics: Conference Series* **551** 012029
[25] Biswas P K, Guguchia Z, Khasanov R, Chinotti M, Li L, Wang K, Petrovic C and Morenzoni E 2015 *Physical Review B* **92** 195122
[26] Cheung Y W, Hu Y J, Imai M, Tanioku Y, Kanagawa H, Murakawa J, Moriyama K, Zhang W, Lai K T, Yoshimura K, Grosche F M, Kaneko K, Tsutsui S and Goh S K 2018 *Physical Review B* **98** 161103
[27] Liu X, Zhang W, Lai K T, Moriyama K, Tallon J L, Yoshimura K and Goh S K 2022 *Physical Review B* **105** 214524
[28] Krenkel E H, Tanatar M A, Kończykowski M, Grasset R, Timmons E I, Ghimire S, Joshi K R, Lee Y, Ke L, Chen S, Petrovic C, Orth P P, Scheurer M S and Prozorov R 2022 *Physical Review B* **105** 094521

[29] Amato A, Luetkens H, Sedlak K, Stoykov A, Scheuermann R, Elender M, Raselli A and Graf D 2017 *Review of Scientific Instruments* **88** 093301
[30] Khasanov R, Guguchia Z, Maisuradze A, Andreica D, Elender M, Raselli A, Shermadini Z, Goko T, Knecht F, Morenzoni E and Amato A 2016 *High Pressure Research* **36** 140–166
[31] Khasanov R 2022 *Journal of Applied Physics* **132** 190903
[32] Andreica D, Marconi D, Khasanov R, Maisuradze A and Amato A 2012 *NMI3 Report*
[33] Maisuradze A, Shengelaya A, Amato A, Pomjakushina E and Keller H 2011 *Physical Review B* **84** 184523
[34] Maisuradze A, Nicklas M, Gumeniuk R, Baines C, Schnelle W, Rosner H, Leithe-Jasper A, Grin Y and Khasanov R 2009 *Physical Review Letters* **103** 147002
[35] Weber M and others 1993 *Physical Review B* **48** 13022–13036
[36] Khasanov R, Karpinski J and Keller H 2005 *Journal of Physics: Condensed Matter* **17** 2453–2460
[37] Brandt E H 2003 *Physical Review B* **68** 054506
[38] Tinkham M 2004 *Introduction to Superconductivity: Second Edition* Dover Books on Physics (Dover Publications) ISBN 978-0-486-43503-9
[39] Carrington A and Manzano F 2003 *Physica C: Superconductivity* **385** 205 – 214
[40] Padamsee H, Neighbor J E and Shiffman C A 1973 *Journal of Low Temperature Physics* **12** 387–411
[41] Kase N, Hayamizu H and Akimitsu J 2011 *Physical Review B* **83** 184509
[42] Hayamizu H, Kase N and Akimitsu J 2011 *Journal of the Physical Society of Japan* **80** SA114
[43] Mitrović B, Zarate H G and Carbotte J P 1984 *Physical Review B* **29** 184–190